PAPER

Check for updates

Sustainable route to antiviral furano-chalcones *via* microwave-assisted solvent-free synthesis with recyclable MgO

Laura Tedesco, [ID] [a] Federico Verdini, [ID] [a] Emanuela Calcio Gaudino, [ID] *[a] Silvia Tabasso, [ID] [a] Irene Arduino,[b] David Lembo,[b] Manuela Donalisio,[b] Giancarlo Cravotto [ID] [a] and Maela Manzoli [ID] *[a]

The increasing demand for sustainable chemical processes has driven the search for renewable feedstocks, environmentally benign catalysts, and energy-efficient methodologies. In this context, we report a solvent-free protocol for the Claisen–Schmidt condensation between biomass-derived furanic aldehydes and acetophenone. Commercial magnesium oxide (MgO) was employed as a recyclable heterogeneous catalyst and subjected to physicochemical characterization and recycling tests to evaluate its stability and reusability. Microwave (MW) irradiation was integrated to ensure rapid and homogeneous heating, leading to enhanced reaction efficiency and reduced processing times. The sustainability of the proposed approach was preliminarily assessed through green chemistry metrics, which confirmed its advantages over conventional methods. The obtained furano-chalcones were investigated for their antiviral potential in *in vitro* cell-based models against common human pathogenic viruses, such as human *herpes simplex virus*, *Zika virus*, *rhinovirus* and *influenza virus*. Their activity was specifically targeted against HSV type 2, highlighting their relevance as pharmacologically active scaffolds and warranting further optimization and investigation. Overall, this work combines renewable resources, recyclable catalysis, and energy-efficient techniques, offering a greener and versatile strategy for the synthesis of high-value bioactive compounds.

Green foundation

1. This paper focuses on the development of sustainable technologies, minimization of hazardous reagents, energy-efficient MW methodologies, integrating recyclable catalysts and renewable feedstock. A solvent-free, MW-assisted Claisen–Schmidt condensation enables rapid and highly selective synthesis of furano-chalcones, that exhibit antiviral activity against HSV-2, demonstrating a dual green-biological significance. Biomass-derived furanic aldehydes are employed. Recyclable commercial MgO acts as an efficient heterogeneous catalyst, maintaining activity and selectivity over six reuse cycles.

2. Superior green metrics (AE, PMI, *E*-factor, EcoScale, Green Motion™) compared to conventional solvent-based methods are attributable to the combination of solvent elimination, recyclable heterogeneous catalysis, and the efficiency of MW heating. When benchmarked against general industrial values, the current methodology clearly outperforms typical laboratory-scale syntheses for waste minimization (*E*-factor <1).

3. Further environmental impact studies through LCA could improve the current research on new antiviral bio-derived moieties.

Introduction

Despite advancements in improving human health, the pharmaceutical industry remains one of the most polluting sectors globally.[1] A 2019 study revealed that the pharmaceutical industry generates approximately 49 tons of CO_2 per million dollars of revenue, surpassing even high-emission industries like automotive manufacturing.[2] While significant efforts have been made toward a greener transition, challenges remain, particularly due to the reliance on toxic fossil-based materials, high energy consumption, and hazardous waste generation.[3,4] In response, the development of more sustainable pharmaceutical compounds and processes is crucial, and chalcones—1,3-diphenyl-2-propen-1-one derivatives—hold promise for both medicinal and environmental innovation.[5] Chalcones are naturally occurring compounds predominantly found in fruits, vegetables, and spices. Nevertheless, limitations associated with the direct use of natural products necessitate synthetic strategies to secure a reliable and scalable supply.[6] Furthermore, naturally derived chalcones are predo-

[a]Department of Drug Science and Technology, University of Turin, Via P. Giuria 9, 10125 Turin, Italy. E-mail: maela.manzoli@unito.it, emanuela.calcio@unito.it
[b]Laboratory of Molecular Virology and Antiviral Research, Department of Clinical and Biological Sciences, University of Turin, Regione Gonzole 10, 10043 Orbassano, Italy

minantly homocyclic and generally exhibit lower bioactivity than synthetic analogues incorporating heteroaryl units, which significantly enhance biological activity. Many organic reactions have been reported in the literature to obtain a wide variety of substituted chalcones that are employed as anticancer, antioxidant, antidiabetic, antibacterial, anthelmintic, antiviral, antifungal and antiprotozoal agents.[7–12] Their ease of absorption and favourable tolerance in humans further enhance their attractiveness for drug development.[13] Beyond therapeutic uses, their π-conjugated planar structure makes them useful as chemical probes, chemosensors, and fluorescent materials in various scientific applications.[14,15] Thus, the structural diversification of chalcones through sustainable synthetic strategies is of considerable interest for pharmaceutical applications. Nowadays, biomass-derived aldehydes such as furfural (FA), 5-methylfurfural (MF), and 5-hydroxymethylfurfural (HMF), obtained through the dehydration of pentoses and hexoses, have attracted growing interest as sustainable and renewable feedstocks for the synthesis of bioactive heteroaryl furano-chalcones.[16] In this context, the transformation of residual lignocellulosic biomass into valuable chemicals through enzymatic and chemical processes offers a promising route to reduce CO_2 emissions, further reinforcing the pivotal role of biomass valorisation in sustainable chemistry.[17] By incorporating furan rings, furano-chalcones enhance the structural and electronic properties of chalcones, expanding their potential for novel biological activities.[18,19] Indeed, furano-chalcones have demonstrated a range of biological effects, including anti-inflammatory,[20] antimicrobial,[21] antifungal[22] and herbicidal[23] activity, as well as inhibition of breast cancer cell proliferation,[24] monoamine oxidase[25] and nitrification.[26]

The Claisen–Schmidt condensation between (hetero)aryl aldehydes and aryl methyl ketones is the benchmark method for accessing chalcones: it is atom-economical, generates water as the sole by-product, and typically furnishes the ε-alkene with high selectivity. Under acid or base catalysis, isolated yields are often moderate (≈50–60%) and substitution-dependent.[27] To improve efficiency, a variety of catalytic systems have been reported—including Brønsted/Lewis acids and recyclable heterogeneous media such as chitosan, Al–Mg hydrotalcites, Cs-pollucite nanozeolites, activated carbons, nanoporous AlSBA-15, cesium salts of heteropolyacids, ionic liquids, mesoporous aluminates, MWCNT–CeO_2 hybrids, modified fluorapatite, Fe_3O_4-MOF core–shells, and $ZnWO_4$ or graphene-supported ZnO nanoparticles—with $BF_3·OEt_2$ often delivering markedly higher yields (≈75–96%) and operational simplicity.[28] Complementary C–C bond-forming strategies broaden access to challenging substitution patterns, including Pd-catalyzed cross-couplings (e.g., Suzuki, Sonogashira, Stille), silver-catalyzed coupling of cinnamic acids with α-keto acids, oxidative carbonylation of boronic acids and styrenes, and Au-nanoparticle-mediated coupling of methyl ketones with aryl alcohols; several systems afford good to high yields and, in heterogeneous formats, catalyst recyclability.[29] While effective, these methods face challenges in catalyst recovery and frequently rely on petroleum-derived solvents, exacerbating their environmental footprint.[22]

In accordance with green chemistry principles, various environmentally friendly approaches have been established. Increasing attention has been devoted to strategies such as recyclable heterogeneous catalysis, solvent-free processes, and unconventional heating techniques.[30] Among them, magnesium oxide (MgO) has emerged as a particularly promising recyclable solid catalyst for Claisen–Schmidt condensation reactions.[31,32] Its catalytic performance is influenced by morphology, particle size and crystallinity, offering advantages such as ease of separation, recyclability, and lower environmental impact compared to traditional methods.[33] Combining MgO catalysis with microwave (MW) heating further amplifies these benefits, as MW irradiation enables rapid and homogeneous energy transfer, leading to shorter reaction times, improved yields, and enhanced selectivity.[34–36] In addition to accelerating chemical transformations, MW-assisted processes have proven highly versatile in organic synthesis and are increasingly employed across a broad spectrum of bond-forming reactions.[37,38] Within this framework, the integration of MW irradiation with MgO catalysis could provide an innovative and sustainable approach to solvent-free chemical processes and holds considerable potential for the efficient synthesis of chalcones and their derivatives.

In this work, a sustainable protocol for the MW-assisted Claisen–Schmidt condensation of biomass-derived furanic aldehydes with acetophenone under solvent-free conditions was described, using commercial magnesium oxide (MgO) as a heterogeneous catalyst. Extended physicochemical characterization, as well as recycling tests, were accomplished to evaluate its stability and reusability. In addition, preliminary assessments of the sustainability of the proposed method were performed by calculating green chemistry metrics. Finally, the obtained furano-chalcones were preliminarily tested for their antiviral activity against common human viruses, aiming to highlight the dual value of this approach in terms of both environmental and pharmacological relevance.

Experimental

Chemicals and reagents

All chemicals and reagents were obtained from commercial suppliers (Sigma-Aldrich, St Louis, MO, USA; Alfa Aesar, Ward Hill, MA, USA) and used without further purification, following the guidelines provided in the respective Safety Data Sheets (SDS). The commercial MgO catalyst (Alfa Aesar) was used in nanopowder form (40–60 nm), with a purity of ≥99% and a specific surface area exceeding 30 m^2 g^{-1}. Commercial Hydrotalcite (HTc) provided by Sigma-Aldrich was also employed for comparison purposes.

General procedure for conventional solvent-free Claisen–Schmidt condensations

Acetophenone (1 mmol), the corresponding aldehydes (FA, MF, HMF and benzaldehyde; 1 mmol), and the catalyst (14 wt% of the total amount of reagents) were combined in a

screw-cap vial containing a magnetic stirring bar. The reactions were performed at 150 °C for 2 h in an oil bath under continuous magnetic stirring. The temperature was maintained and monitored using a hotplate stirrer CC162 and a temperature controller SCT1 (Stuart®, Bibby Scientific Ltd, Stone, Staffordshire, UK).

General procedure for MW-assisted solvent-free Claisen–Schmidt condensations

MW-assisted reactions were carried out in a multimode reactor (SynthWave, Milestone Srl, Bergamo). The instrument features a high-pressure stainless-steel chamber capable of operating at temperatures up to 300 °C and pressures up to 199 bars. Acetophenone (1 mmol), corresponding aldehydes (1 mmol) and catalyst (MgO or HTc, 14 wt% of the total amount of reagents) were placed inside a quartz vial and heated (90, 120, 150, 180 °C) by MW irradiation, under an inert atmosphere (N_2) and magnetic stirring (300 rpm), for 2 h. Upon completion of the reaction and cooling, the reaction mixture was dissolved in 5 mL of ethyl acetate (EtOAc) and filtered under vacuum to recover the catalyst, which was washed twice with 2.5 mL of EtOAc. The recovered solution was then dried under vacuum and analysed *via* gas chromatography-mass spectrometry (GC-MS), while the MgO catalyst was transferred to a crucible and calcined in a muffle furnace (Nabertherm GmbH, Lilienthal, Germany) at 450 °C for 2 h with a 50-minute heating ramp to remove organic residues. GC-MS analyses were performed on an Agilent Technologies 6850 Network GC System (Agilent Technologies, Santa Clara, CA) equipped with a 5973 Network Mass Selective Detector and a 7683B Automatic Sampler, using a capillary column (HP-5MS; length 30 m; i.d. 0.25 mm; film thickness 0.25 μm). In detail, for the GC-MS analysis, the oven temperature program was set as follows: initial temperature of 50 °C for 5 min, ramped to 100 °C at 10 °C min^{-1} for 1 min, ramped to 230 °C at 20 °C min^{-1} for 1 min, ramped to 300 °C at 20 °C min^{-1} for 5 min, and held for 15 min. The injector temperature was set at 250 °C, with a split ratio of 20 : 1. Helium was used as the carrier gas at a constant flow rate of 24 mL min^{-1}. The conversion of ketone to furano-chalcone ($X_{\text{furano-chalcone}}$%), the yield of furano-chalcone ($Y_{\text{furano-chalcone}}$%) and the selectivity to furano-chalcone ($S_{\text{furano-chalcone}}$%) were calculated according to eqn (1)–(3), respectively.

$$X_{\text{furano-chalcone}}(\%) = \frac{([\text{KET}]_i - [\text{KET}]_t)}{[\text{KET}]_i} \times 100 \quad (1)$$

$$Y_{\text{furano-chalcone}}(\%) = \frac{n_y}{n_t} \times 100 \quad (2)$$

$$S_{\text{furano-chalcone}}(\%) = \frac{n_y}{n_i - n_t} \times 100 \quad (3)$$

Selectivity was defined as the fraction of converted ketone forming the desired chalcone product. The ketone was used as the reference reactant, as aldehydes in Claisen–Schmidt condensations are prone to side reactions such as self- or polycondensation.[39]

Furano-chalcones purification for subsequent biological assay was carried out by Flash-Chromatography using a PuriFlash® 5.050 system (Interchim, Montluçon, France). The separation was performed on C18 packed columns (12 g; Daily purity, Sepachrom srl, Rho, Milan) at a flow rate of 15 mL min^{-1}. Before purification, 0.2 g of each crude sample were mixed with 0.5 g of C18 silica and packed into a precolumn. A gradient elution was employed using distilled water (A) and methanol (B), as detailed in Table S1 of the SI. The purified chalcones (**3a**, **3b**, **3c** and **3d** in Scheme 1) were then analysed by GC-MS (Fig. S1–S4 of the SI) and NMR (^{1}H-NMR and ^{13}C-NMR), using a Jeol JNM-ECZ600R spectrometer (Jeol, Tokyo, Japan) operating at a frequency of 600 MHz (Fig. S5–S12 of the SI).

Catalyst characterization

Powder X-ray diffraction (PXRD). Patterns were collected with a PW3050/60 X'Pert PRO MPD diffractometer from PANalytical working in Bragg–Brentano geometry, using as a source the high-powered ceramic tube PW3373/10 LFF with a Cu anode (using Cu K$_{\alpha 1}$ radiation λ = 1.5406 Å) equipped with a Ni filter to attenuate K$_{\beta}$. Scattered photons were collected by a real time multiple strip (RTMS) X'celerator detector. Data were collected in the 10° ≤ 2θ ≤ 90° angular range, with 0.02° 2θ steps. The powdered samples were examined in their as-received form and posed in a spinning sample holder to minimize preferred orientations of crystallites.

Field emission scanning electron microscopy (FESEM). Measurements were carried out using a TESCAN S9000G FESEM 3010 microscope (30 kV), equipped with a high brightness Schottky emitter and Energy Dispersive X-ray Spectroscopy (EDS) analysis thanks to a Ultim Max Silicon Drift Detector (SDD, Oxford, Abingdon-on-Thames, UK). The samples were observed in their as-prepared forms without any metallization, whereas those after MW-assisted Claisen Smith condensation of aldehyde (reaction conditions: 150 °C, 2 h) were submitted to metallization with Cr (*ca.* 5 nm) to avoid any charging effect due to the possible presence of reaction products and intermediates at the surface of the used catalyst (Emitech K575X sputter coater). MgO nanoparticle size distributions were obtained by considering for each sample a representative number of nanoparticles in the images and the mean particle diameter (d_m) was calculated by applying the following equation: $d_m = \sum d_i n_i / \sum n_i$, being n_i the number of nanoparticles with diameter d_i. Before the measurements, the samples were deposited on a stub that was coated with a conducting adhesive and inserted into the chamber in a fully motorized procedure.

Thermogravimetric analysis (TGA). Analyses were carried out using a TGA 4000 Thermogravimetric Analyzer (PerkinElmer, Inc., Waltham, Massachusetts, USA) to evaluate the presence of organic residues on the MgO catalyst before and after calcination. In a standard procedure, approximately 8 mg of sample were placed in a crucible within the furnace. The temperature was initially set to 30 °C and maintained for 1 minute, then increased to 800 °C at a heating rate of 10 °C min^{-1}.
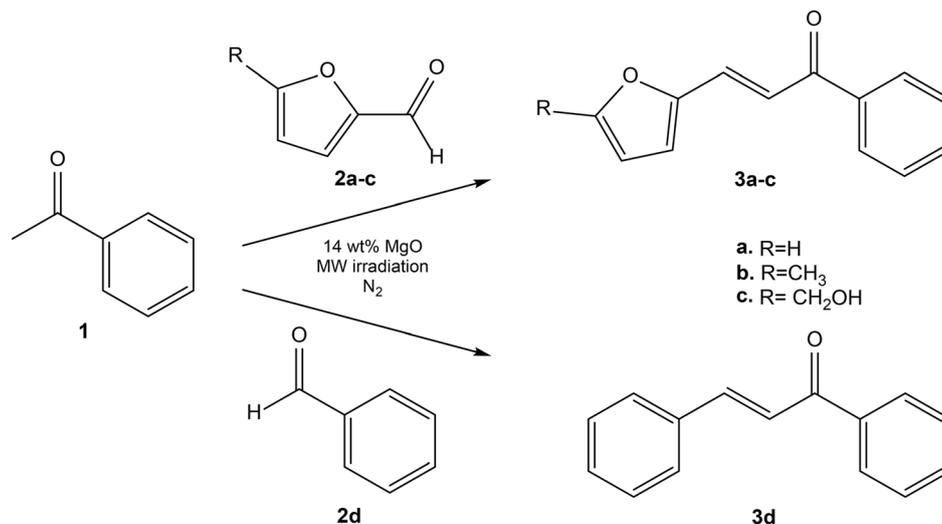
Scheme 1 Solvent-free MW-assisted Claisen–Schmidt condensation of acetophenone **1** with furanic aldehydes **2a–c** and benzaldehyde **2d** over MgO.

Green metrics calculation

Atom economy (AE), molar efficiency (ME), process mass intensity (PMI), and E-factor have been calculated according to literature,[40] applying the following equations:

$$AE = \frac{\text{number of atoms in the final products}}{\text{number of atoms in the reagents}} \quad (4)$$

$$ME = \frac{\text{moles of products}}{\text{moles of reagents} + \text{moles of catalyst}} \times 100 \quad (5)$$

$$PMI = \frac{\text{total mass of process steps}}{\text{mass of product}} \quad (6)$$

$$E\text{-factor} = \frac{\text{mass of total waste}}{\text{mass of product}} \quad (7)$$

Evaluation of biological activity: cytotoxicity and antiviral assays

Cell lines and viruses. African green monkey kidney cells (Vero, ATCC® CCL-81™), human cervix adenocarcinoma epithelial cells (HeLa, ATCC® CCL-2™), Madin–Darby canine kidney cells (MDCK, ATCC® CCL-34™), human lung fibroblast cells (MRC-5, ATCC® CCL-171™) and human foreskin fibroblast (HFF-1, ATCC® SCRC-1041) were grown as monolayers in Dulbecco's modified Eagle's medium (DMEM) (Sigma-Aldrich, St Louis, MO), supplemented with 10% heat inactivated fetal bovine serum (FBS) (Gibco, Waltham, MA) and with 1% (v/v) antibiotic–antimycotic solution (Sigma-Aldrich) in humidified 5% CO_2 atmosphere at 37 °C. The *herpes simplex virus* type 2 strain (HSV-2, ATCC® VR-540) and the *Zika virus* 1947 Uganda MR766 (ZIKV)[41] were propagated on Vero cells. *Human rhinovirus* type A1 (HRV, ATCC® VR-1559) was produced on HeLa cells. *Influenza virus* type A strain H1N1 (IFV-A H1N1; strain A/ California/07/2009 (H1N1) pdm09; ATCC® VR-1894™) was propagated on MDCK cells in DMEM containing 1 µg mL^{-1} of IX-

type porcine pancreatic trypsin (Sigma-Aldrich). Virus titration by means of immunocytochemistry is detailed in the SI.

Cell viability assay. The effect on cell viability of compounds was evaluated *via* the MTS [3-(4,5-dimethylthiazol-2-yl)-5-(3-carboxymethoxyphenyl)-2-(4-sulfophenyl)-2H-tetrazolium] assay, using the Cell Titer 96 Proliferation Assay Kit (Promega, Madison, WI) as described elsewhere.[42]

Virus inhibition assay. The antiviral activity of the compounds was investigated *via* plaque (for HSV-2) or focus (for ZIKV, HRV and IFV) reduction assays. Briefly, sub-confluent cells seeded in 96-well plates were pre-treated with serial dilutions of compounds (40 to 0.6 µg mL^{-1}) for 2 h. Afterwards, infection was performed with a fixed viral inoculum (multiplicity of infection, MOI: 0.01 for ZIKV, HRV, IFV; 0.001 for HSV-2). ZIKV-, HRV- and IFV-infected cells were incubated for 24 h and then subjected to indirect immunocytochemistry as outlined in the SI. On the other hand, for HSV-2-infected cells, the viral inoculum was removed after 2 h and serial dilutions of compounds in medium containing 1.2% methylcellulose were added to cells for 24 h; afterwards, crystal violet staining was performed. Infected foci/plaques were quantified, and viral infectivity was reported as the mean percentage of the treated samples compared to the untreated control.

Results and discussion

MW-assisted solvent-free Claisen–Schmidt condensation

As an attempt to develop a sustainable synthetic route to furano-chalcones, solvent-free Claisen–Schmidt condensations of acetophenone (**1**) with both bio-derived furanic aldehydes (**2a–c**) and benzaldehyde (**2d**) (used as benchmark) were carried out under MW irradiation in the presence of MgO as heterogeneous catalyst (Scheme 1). Unlike many reported pro-

tocols that rely on engineered nanostructures or catalyst pre-treatment,[43–48] the method reported in this work employs unmodified and commercially available MgO. As previously reported,[49] the base-catalysed Claisen–Schmidt condensation typically proceeds through enolate formation, carbon–carbon bond formation, and subsequent dehydration to afford α,β-unsaturated carbonyl compounds. Nanostructured MgO, characterized by high surface area and abundant basic sites, enhances catalytic activity, selectivity, and reusability. The catalytic process is mainly driven by Lewis basic O^{2-} sites, which are strong enough to deprotonate the α-hydrogens of the ketone to form the enolate ion, thereby forming a surface-adsorbed enolate intermediate (stabilized carbanion).[50,51] The Claisen–Schmidt condensation is, in principle, a formally atom-economic route to chalcones, as the ideal stoichiometric transformation releases water as the sole by-product. In practice, however, competitive pathways such as ketone or aldehyde self-condensation, Michael addition, Cannizzaro disproportionation of aromatic aldehydes, and the formation of insoluble polymeric ("humin-like") materials may occur under the basic or acidic conditions commonly employed.[52–54] These side reactions generate additional by-products and substantially reduce the effective atom economy of the process. Moreover, in Claisen–Schmidt condensations, aldehyde conversion is often used as the primary metric to assess reaction progress. However, aldehydes—particularly biomass-derived ones—are prone to degradation and polymerization, which can artificially inflate conversion values and lead to a misleading assessment of catalytic efficiency.[55] Accordingly, in this work, the conversion of the ketone was taken as the reference parameter to provide a more reliable evaluation of catalytic performance of MgO. To establish an efficient and green protocol for the synthesis of furano-chalcones, a solvent-free Claisen–Schmidt condensation was investigated under MW irradiation using commercial MgO as heterogeneous catalyst.

MW irradiation was selected to ensure homogeneous volumetric heating and precise temperature control under solvent-free conditions, prioritizing selectivity and reproducibility over reaction time minimization.[56] The initial objective was to evaluate the influence of reaction temperature since this para-meter is known to strongly affect both conversion and selectivity in solid-state condensations.

A systematic screening of reaction temperature and time was carried out under controlled MW heating to identify the optimal conditions for the solvent-free MW-assisted Claisen–Schmidt condensation, maximizing catalytic performance while maintaining high selectivity toward the desired furano-chalcones. The complete pre-screening dataset, including temperature (90–180 °C) and reaction time (1.5–2 h) for all substrates, is reported in the SI (Table S2). As summarized in Table 1, increasing the reaction temperature from 150 °C to 180 °C resulted in higher substrate conversions. In particular, for MF and HMF, conversion increased from 63% to 83% (Table 1, entries 3 and 4) and from 90% to 99% (entries 6 and 7), respectively. Similarly, as for FA, conversion was enhanced at 180 °C. However, among the synthesized compounds, product **3c** is of particular interest, since HMF stands out among the key compounds derivable from lignocellulosic biomass, representing a high-value, renewable, and extensively utilized chemical,[57] particularly promising for energy-efficient, low-temperature catalytic processes.[58] Furthermore, 5-HMF can be obtained from the MW-assisted conversion of C-6 sugars.[59,60] Therefore, warranting particular attention to the reaction conditions employed for this compound, an improved selectivity toward **3c** was instead obtained at 150 °C (Table 1, entry 6), with a selectivity of 93% compared to 86% at 180 °C (Table 1, entry 7). An exception was observed for the bench-mark product **3d**: despite the selectivity remained constant (100%) when increasing the temperature from 120 °C to 150 °C, the conversion improved from 13% to 59% (Table 1, entries 8 and 9 respectively), resulting in a proportional increase in yield. Additional experiments were carried out at 90 and 120 °C on furfuryl-based aldehydes. At 90 °C, no substrate conversion was observed, conversely the increase of temperature to 120 °C resulted in measurable conversion only for HMF (Table 1, entry 5), while both FA and MF remained unreactive, underscoring HMF reactivity under mild thermal conditions,[61] likely arising from the electron-deficient nature of the furan ring and the activated aldehyde group.

Table 1 MW assisted, solvent free conversion and selectivity of MgO catalyzed Claisen−Schmidt condensations[a]

Entry	Ketone	Aldehyde	Product	Temp. (°C)	Conv.[b] (%)	Sel. (%)	Yield[c] (%)
1	**1**	FA (**2a**)	**3a**	150	51	100	51
2				180	65	99	64
3		MF (**2b**)	**3b**	150	63	99	63
4				180	83	99	83
5		HMF (**2c**)	**3c**	120	69	94	65
6				150	90	93	84
7				180	99	86	85
8		Benzaldehyde (**2d**)	**3d**	120	13	100	13
9				150	59	100	59
10				180	79 (99)[d]	98 (100)[d]	77 (99)[d]
11		Benzaldehyde[e]		180	70	99	69

[a] Reaction conditions: acetophenone (1 mmol), aldehyde (1 mmol), MgO 14 wt% stirred for 2 h and heated to the respective temperature. [b] Conversion is referred to ketone (see Experimental section). [c] Determined by GC-MS. [d] Reaction performed in EtOH. [e] HTc 14 wt% used as catalyst instead of MgO.

Moreover, the scalability of the solvent-free MW-assisted protocol was preliminarily evaluated by a threefold increase in reaction scale, as detailed in the SI (Table S3). The MgO catalyst was next compared with hydrotalcite (HTc) under the optimized solvent-free MW-assisted conditions. HTc, an inexpensive and commercially available layered double hydroxide, is widely employed as a heterogeneous base in organic reactions, thanks to its tuneable, moderate basicity.[62–64] Under identical reaction conditions, MgO outperformed HTc in terms of conversion (Table 1, entries 10 and 11). In addition, HTc exhibited poor stability, its recovery by filtration was difficult or impossible, likely due to delamination under MW irradiation and exposure to water produced during reaction. By contrast, MgO was easily separated after the reaction. The proposed microwave-assisted solvent-free protocol is highly tunable, allowing even less reactive substrates to be efficiently converted by appropriate selection of the reaction temperature. Although the use of ethanol resulted in a marginal increase in ketone conversion (Table 1, entry 10), solvent-free conditions were selected for further optimization. This choice was motivated by the need to maximize process safety—by avoiding pressurized systems at 150 °C—and to comply with green chemistry principles through the minimization of solvent use, waste generation, and energy-intensive solvent recovery steps.

Conventional heating *vs.* MW-heating

A direct comparison between conventional and MW heating under identical conditions (150 °C, 2 h, 14 wt% MgO, solvent free) highlighted significant advantages of MW irradiation. For all furanic aldehydes, MW heating afforded higher conversions (Fig. 1), thanks to its volumetric, homogeneous heating profile that minimizes thermal gradients and promotes dipolar polarization of intermediates, stabilizing transition states and generating local hot spots that boost catalyst activation.[65,66] Product selectivity remained essentially complete, except for a slight drop for HMF-derivative **3c** (99% → 93%) (Fig. 1).

In contrast, benzaldehyde exhibited poorer performance under MW heating. Its lower dielectric constant likely prevents efficient MW absorption and hot spot formation, while its reduced polarity weakens adsorption onto basic O^{2-} sites of MgO.

As a result, both substrate and catalyst may absorb less energy, carbonyl activation could be hindered, and benzaldehyde conversion falls below that achieved with conventional heating.[67,68]
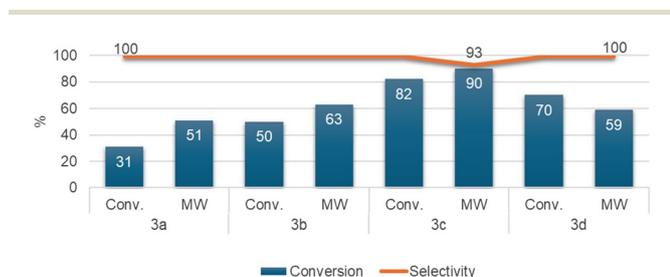
Catalyst recyclability

To assess the stability and recyclability of the MgO catalyst, six consecutive reaction cycles were performed using fresh substrates under the optimized conditions (150 °C, 2 h).

Catalyst recovery rates ranged from 71% to 95%, depending on substrates and cycle number, with an average recovery of 86%. While simple washing with acetone and EtOAc led to a decline in activity (data not shown), a calcination step at 450 °C between cycles restored or even increased the catalytic activity (Fig. 2). The yields remained high for five consecutive cycles before a slight drop was observed after the sixth run.

To get more insights on this activity trend, both morphology and structure of the MgO catalyst before reaction and over multiple reaction cycles in the presence of the best HMF substrate were investigated by FESEM and XRD.

Firstly, MgO nanoparticles with globular shape and size ranging between 10 and 50 nm, resulting in a mean diameter of 35.4 ± 14.4 nm, were observed before reaction (Fig. 3A, A′ and S13). The corresponding XRD pattern (Fig. 3E, red line and Fig. 3F, red line) shows well defined and quite intense peaks related to the cubic crystalline phase of MgO along with very weak peaks due to hexagonal $Mg(OH)_2$. It is worth noting that the structure of the catalyst before reaction was overall retained after calcination at 450 °C, as revealed by the small increase in crystallinity of cubic MgO nanoparticles (Fig. 3E, black curve). Conversely, as for the morphology, nanoparticles with size comparable to those observed on the catalyst before calcination were accompanied by larger particles ranging between 100 and 300 nm (Fig. S14). However, the size of the MgO nanoparticles decreased after the first reaction cycle followed by calcination at 450 °C, resulting in a mean diameter of 16.2 ± 4.3 nm (Fig. 3B and B′) and remained essentially constant through cycles 2–5, being the average size equal to 16.7 ±

Fig. 1 Comparison of MW and conventional (conv.) heating in the synthesis of compounds **3a–d** (150 °C, 2 h).
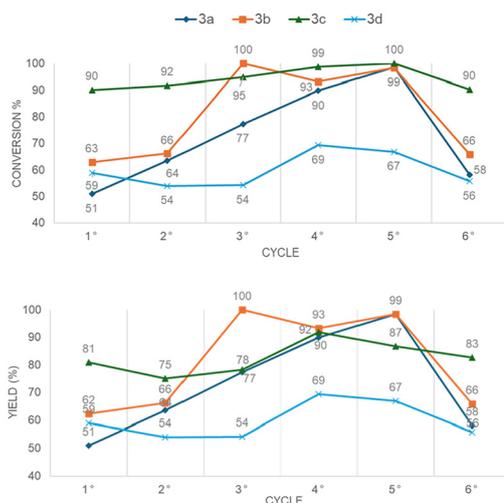

Fig. 2 Catalytic performance of MgO over six consecutive cycles under optimized MW-assisted solvent-free conditions (150 °C, 2 h). Catalyst activity was restored or enhanced by intermediate calcination to 450 °C between cycles.
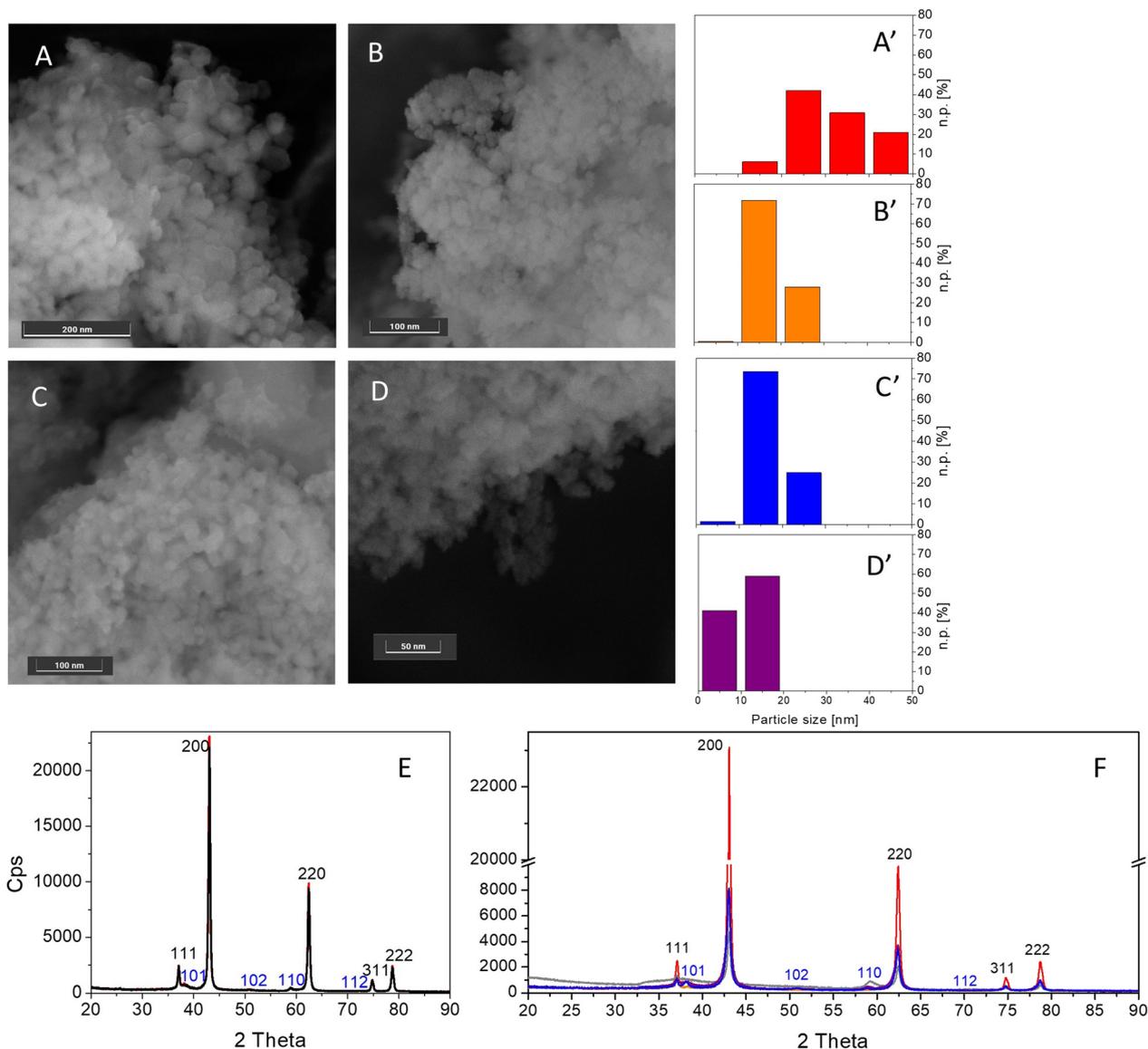
Fig. 3 FESEM representative In-Beam UH-Resolution SE images and particle size distributions of the MgO catalyst before reaction (A, A′) and after the first (B, B′), fifth (C, C′) and sixth (D, D′) reaction cycle followed by calcination at 450 °C using HMF as substrate. Instrumental magnification: 457 000×, 600 000×, 858 000× and 943 000×. Comparison between the XRD patterns of MgO before reaction (red line) and after calcination at 450 °C (black line) (E). Comparison among the XRD patterns of MgO before reaction (red line), after the first (orange line), fifth (blue line) and sixth (purple line) reaction cycle followed by calcination at 450 °C using HMF as substrate (F). The XRD pattern collected after the sixth cycle without any calcination step at 450 °C is reported for comparison (grey line). Black Miller indexes: cubic MgO (00-003-0998), blue Miller indexes: hexagonal Mg(OH)$_2$ (00-001-1169).

3.5 nm in cycle 5 (Fig. 3C and C′), with a further reduction to 11.1 ± 2.9 nm in cycle 6 (Fig. 3D and D′).

Accordingly, the diffraction peaks related to cubic MgO after the first, fifth and sixth runs (Fig. 3E, orange, blue and purple lines) are markedly lower in intensity with respect to the XRD pattern of the catalyst before reaction (red line) and have similar intensity. Conversely, some crystalline Mg(OH)$_2$ is formed during reaction, as demonstrated by the peaks observed for the catalyst after the sixth reaction cycle without any calcination step (grey line). These peaks, detected after the first, fifth and sixth runs never exceeded in intensity those

observed before reaction, pointing out that MgO is effectively reactivated upon calcination at 450 °C. In this frame, the decrease in size and crystallinity during the catalytic runs may account for particle erosion due to the formation of water as co-product, which promotes the growth of a Mg(OH)$_2$ layer on the surface of the catalyst during reaction that is converted to MgO upon calcination at 450 °C. As a consequence, gradual fragmentation of the nanoparticles occurs, ultimately compromising the catalyst performance. A similar catalytic trend was previously reported for MgO nanoparticles prepared under MW irradiation and tested in the MW-assisted formylation of

amines with formic acid.[69] The authors ascribed the decrease in activity observed at the fourth run to moisture absorbed on the catalyst surface. The presence and evolution of hydroxyl species are critical for MgO efficiency in Claisen–Schmidt condensations. Controlled surface hydroxylation can enhance catalytic activity by reducing activation barriers for enolate formation and proton transfer, as Brønsted –OH groups synergistically complement exposed O^{2-} sites by weakening overly strong intermediate binding. However, hydration beyond the optimal threshold leads to competitive water adsorption, surface saturation of –OH groups, and a marked decrease in turnover frequency.[70,71] These findings are further supported by studies on engineered MgO systems, where structural design strategies that regulate water adsorption have been shown to enhance surface basicity, porosity, and active site dispersion.[72,73] Calcination is therefore essential to remove excess $Mg(OH)_2$-like terminations that block active sites, and to effectively restore catalytic activity.[74,75] Upon calcination at 450 °C, spent MgO regained its crystallinity, as evidenced by

the disappearance of hydroxide-related reflections in the XRD pattern and the absence of impurity peaks (Fig. 3E). However, after the sixth run the XRD analysis of the not calcined catalyst revealed peak broadening and attenuation indicative of surface deactivation, likely due to surface hydration and/or accumulation of organic residues. This was further supported by performing TGA measurements of the MgO catalyst before reaction (Fig. 4A), which accounts for a 12.97% weight loss and after the sixth reaction cycle followed by calcination at 450 °C using benzaldehyde as the less reactive substrate among the tested aldehydes (Fig. 4B), which shows similar weight loss (12.97%) and indicating effective removal of organic residues around 315 °C. Significant weight loss (40.64%) was observed at 362 °C after the sixth catalytic run without any calcination step at 450 °C (Fig. 4C), confirming the presence of adsorbed organic matter on the catalyst surface after use. Interestingly, differently from what observed for HMF, XRD analyses clearly show quite intense peaks due to $Mg(OH)_2$ after the sixth reaction cycle using benzaldehyde as substrate (Fig. 4D, grey line).
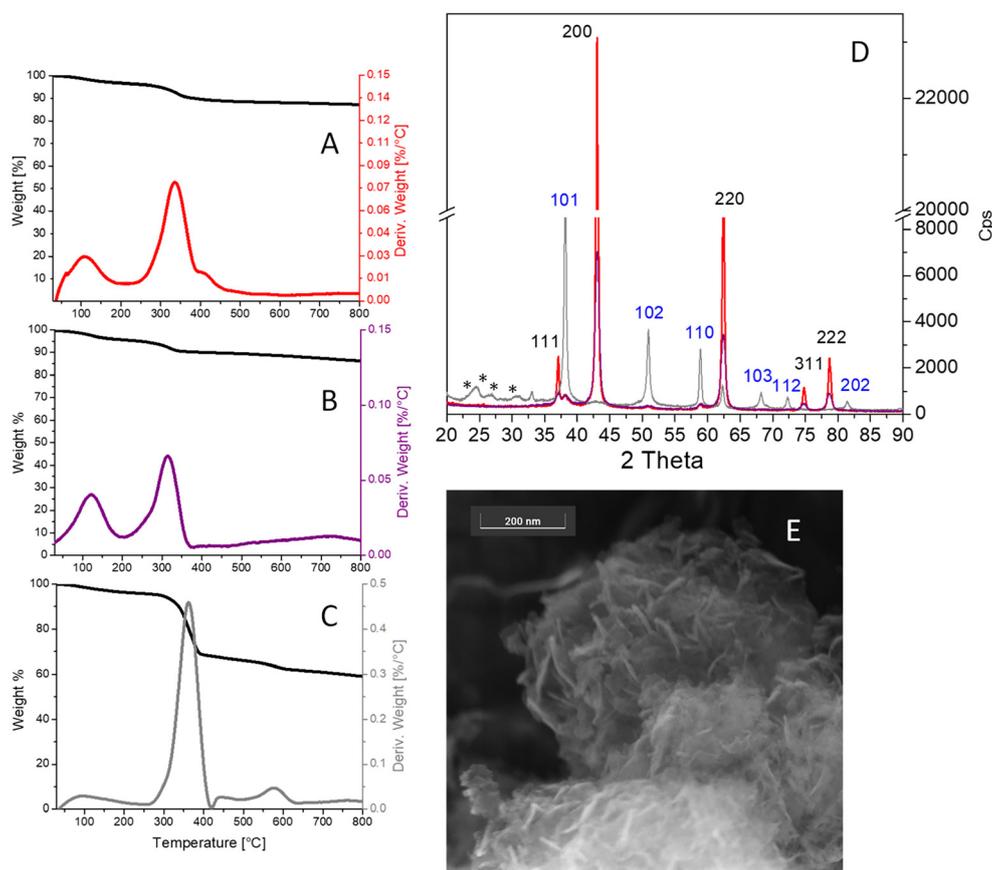

Fig. 4 Thermo-gravimetry (TG) and differential thermo-gravimetry (DTG) curves of the MgO catalyst before reaction (A) after the sixth reaction cycle followed by calcination at 450 °C using benzaldehyde as substrate (B) and after the sixth cycle without any calcination step at 450 °C (C). XRD patterns of the MgO catalyst before reaction (red line) after the sixth reaction cycle followed by calcination at 450 °C using benzaldehyde as substrate (purple line) and after the sixth cycle without any calcination step at 450 °C (grey line) (D). Black Miller indexes: cubic MgO (00-003-0998), blue Miller indexes: hexagonal $Mg(OH)_2$ (00-001-1169). Asterisks: monoclinic benzoic acid (00-001-0596). FESEM representative In-Beam UH-Resolution SE image of the MgO catalyst and after sixth reaction cycle using benzaldehyde as substrate without any calcination step at 450 °C (E). Instrumental magnification: 450 000×.

In addition, at lower 2 Theta peaks possibly due to unreacted benzaldehyde and/or benzoic acid adsorbed on MgO are also observed further indicating that if not subjected to thermal regeneration, the combined effect of rehydroxylation and persistent organic fouling would progressively deactivate the catalyst. Benzaldehyde can be adsorbed on the MgO surface by abstracting the aldehydic H.[76] The authors proposed that the two benzoate species observed by *in situ* FTIR spectroscopy can also be produced by breaking the C=O bond. These species are stable under N_2 flow and do not react with the employed 2-hydroxyacetophenone in the liquid-phase Claisen–Schmidt condensation. These features explain the observed benzaldehyde recalcitration towards the reaction with respect to the other substrates. FESEM characterization also confirms the presence of $Mg(OH)_2$ elongated crystals covering the surface of MgO (Fig. 4E).[69] When calcination is applied before each reaction cycle, the surface is restored to a predominantly oxide state. Nevertheless, the slight decline in activity observed in the sixth cycle is likely due to cumulative nanostructural deterioration (*e.g.* irreversible particle fragmentation) that cannot be fully reversed through thermal treatment.

Green chemistry assessment

To assess the greenness of the optimized protocol (150 °C, 2 h), different green metrics were calculated for each product (**3a**–**3d**), including atom economy (AE), mass efficiency (ME), process mass intensity (PMI) and *E*-factor. These values are reported in Table 2 (see also the SI). The green chemistry metrics calculated for compounds **3a**–**3d** confirm the sustainability of the developed protocol. Atom economy values were consistently high (0.92–0.93), reflecting the intrinsic efficiency of the Claisen–Schmidt condensation. Mass efficiency was more variable, with compound **3c** showing the highest value (29.3%), in line with its superior yield. Similarly, the process mass intensity and *E*-factor values were lowest for **3c** (1.47 and 0.28, respectively), underscoring the reduced waste generation and improved material utilization associated with this substrate.

The other chalcones (**3a**, **3b**, **3d**) also displayed favourable PMI (1.98–2.44) and *E*-factor values (0.75–1.14). These results

indicate minimal waste generation and efficient material utilization, fully consistent with the principles of green chemistry. It should be noted that the literature offers only very limited quantitative data on sustainability indicators for these reactions, with most reports focusing exclusively on yield and reaction time. This gap highlights the lack of systematic evaluation of green parameters in traditional Claisen–Schmidt methodologies. For the sake of comparison, one of the few available studies reporting an *E*-factor for both a solution-phase and solvent free reaction was considered. Abid *et al.*[77] calculated an *E*-factor of 560 for a solution-phase reaction (ethanol, 50 °C, 2 h, multi-step workup, 47% yield), whereas a mechanochemical ball-milling approach reduced the value to 293 under otherwise comparable conditions (86% yield, 60 min). In contrast, the present solvent-free MW-assisted MgO protocol afforded *E*-factors as low as 0.28, thus reducing waste generation by three orders of magnitude relative to conventional conditions. Taken together, these results confirm that the proposed method not only delivers high selectivity but also establishes a highly sustainable route to furano-chalcones. The Green Motion™ radar plots[78] (Fig. 5) emphasize the protocol effectiveness in solvent elimination and toxicity reduction through the removal of corrosive NaOH and explosive EtOH. By employing bio-based starting materials, the process achieves notable sustainability improvements. While operating under nitrogen pressure lowers the Process Green Motion™ score to 60, the overall score rises from 70 to 80, confirming its enhanced environmental performance. The metric, however, does not account for catalyst recyclability or other factors that could further improve the process sustainability. The EcoScale assessment was employed to further validate the sustainability of the proposed protocol, integrating considerations of yield, safety, operational simplicity, and ease of purification.[79] Considering that the ideal EcoScale value for a reaction is 100, the EcoScale scores of the synthesized furano-chalcones (**3a–c**), as illustrated in Fig. 6, are consistently higher than that of the classical Claisen–Schmidt condensation carried out in ethanol with NaOH as homogeneous catalyst (EcoScale = 61).[80] Compound **3a** achieved a score of 65, while significantly higher values were obtained for **3b** (74.5) and **3c** (75). The reduced performance of the classical approach is mainly due to the use of hazardous reagents such as NaOH and HCl (for the reaction work up), coupled with more demanding purification steps. By contrast, the solvent-free, MW-assisted proposed procedure benefits from the use of a recyclable heterogeneous catalyst (MgO) and simplified handling, resulting in markedly improved EcoScale scores.

Notably, the highest score was achieved for compound **3c** (EcoScale = 75), which is especially relevant in view of the scope of this study. Overall, the EcoScale analysis corroborates the superior greenness and practicality of the present methodology when compared with conventional solvent-based Claisen–Schmidt condensations.

In order to better emphasize the competitiveness of the newly developed solvent-free and MW-assisted protocol, the Green Star metric, grounded in the twelve principles of Green

Table 2 Green metrics for the developed MW-assisted solvent-free Claisen–Schmidt condensation

Process	Chalcone	AE	ME (%)	PMI	*E*-factor	Ref.
MW-assisted, (solvent free, MgO)	**3a**	0.92	18.5	2.44	1.14	This work
	3b	0.92	22.3	1.98	0.75	
	3c	0.93	29.3	1.47	0.28	
	3d	0.92	21.1	2.10	0.84	
Ball-mill, (solvent free, KOH)	**3d** analogue	n.d.	—	—	293	72
Conventional, solution-phase (EtOH, NaOH)	**3d** analogue	n.d.	—	—	560	

Fig. 5 Green Motion™ radar plots comparing the environmental profile of the traditional Claisen–Schmidt condensation (upper panel) and the developed MW-assisted solvent-free protocol (lower panel).
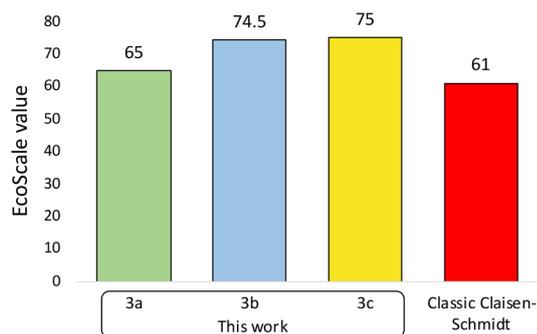

Fig. 6 EcoScale values calculated for the presented solvent-free MW-assisted reactions and for the classic Claisen–Schmidt condensation (yields: **3a–c** = experimental; classic Claisen–Schmidt = 100%).

Chemistry, was employed.[81] Despite the high temperature and consumption, the Green Star metric highlights the "greener" nature of the proposed protocol (Fig. 7). This metric visually demonstrates the trade-offs inherent in the methodology: while the energy efficiency (Principle 6) reflects the use of 150 °C, this is vastly outweighed by the maximum scores achieved in waste prevention (P1), Less Hazardous Synthesis (P3), Safer Solvents (P5), Catalysis (P9), Safety (P12). Details on Green Star Calculation Parameters have been included in the SI.
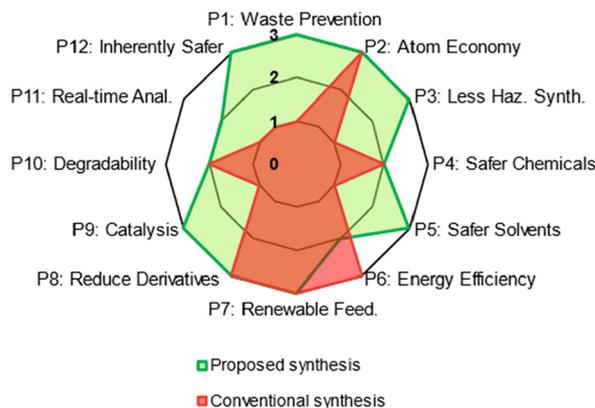

Fig. 7 Green star score for the MW-assisted and solvent-free proposed protocol.

Biological activity

Over the last two decades, the chalcone scaffold has emerged as a promising antiviral chemical entity, and several studies have reported activity of chalcones against members of various viral families, such as the *Herpesviridae* family, specifically HSV-1, HSV-2 and HCMV.[82–85] Beyond herpes viruses, chalcones have been investigated for activity against a broader panel of viral pathogens.[86] Notably, a recent synthetic series of chalcone derivatives demonstrated inhibition of multiple RNA viruses (including *e.g. Zika virus*, *La Crosse virus*, and *Human coronavirus* OC43) with low cytotoxicity.[87] Other reports document chalcone derivatives inhibiting influenza neuraminidase with an EC_{50} 27.63 μM and 28.11 μM for IFV-A H5N1 and IFV-A-H1N1 respectively,[88] *Dengue Virus* NS5 protein,[89] and the human immunodeficiency virus with an EC_{50} of 0.022 μg mL^{-1} and a good therapeutic index (TI = 489).[90] These reports suggest that the chalcone core is endowed with broad-spectrum antiviral activity, pointing to a possible antiviral effect of furano-chalcones herein synthesized.

In this study, we aimed firstly to assess the possible anti-proliferative effect of the furano-chalcones, since a high cytocompatibility is an essential parameter in biological applications based on cell models. The results of the cell viability assay, depicted in Table S6, showed a high cytocompatibility for compounds **3a–c**, while compound **3d** showed a marked cytotoxic effect on all cell lines used, thus excluding the compound from further biological analysis.

Based on these results, the antiviral activity of compounds was evaluated at non-cytotoxic concentrations, to rule out that the antiviral effect could be due to cellular toxicity. The inhibitory effect of furano-chalcones was evaluated against different human viral pathogens, commonly spread worldwide and cause of disease in humans. Viruses were selected for the different route of transmission (*i.e.*, sexual for HSV-2, arthropod-borne for ZIKV, and respiratory for HRV and IFV-A). Results in Table 3 show that all furano-chalcones inhibited HSV-2 in a dose-dependent manner, whereas compounds were inactive against ZIKV, HRV, and IFV-A (Fig. S15). The selectivity

Table 3 Anti-HSV-2 efficacy of compounds

Compound	$EC_{50}{}^a$ (μg mL^{-1}) (95% CI^b)	$CC_{50}{}^c$ (μg mL^{-1}) (95% CI^b)	SI^d
3a	5.8 (4.9 to 7.1)	44.1 (39.2 to 49.5)	7.6
3b	6.6 (5.3 to 8.2)	37.7 (32.1 to 41.0)	5.7
3c	10.2 (9.1 to 12.4)	93.0 (82.3 to 100.2)	9.1

^{a} EC_{50}: half maximal effective concentration. ^{b} CI: 95% confidence interval. ^{c} CC_{50}: half maximal cytotoxic concentration. ^{d} SI: selectivity index.

index (SI) is a parameter that characterizes the antiviral efficacy of a compound, expressed as its relative efficacy in inhibiting viral replication compared to its cytotoxicity. As outlined in Table 3, the best SI (9.1) was obtained for compound **3c**, due to its higher cytocompatibility compared to the other two compounds. Altogether, our study is the first, to the best of our knowledge, to report the antiviral activity of furano-chalcones, highlighting the potential of this subclass of chalcones to serve as antiviral scaffolds.

Conclusions

A solvent-free and MW-assisted protocol for the Claisen–Schmidt condensation of biomass-derived furanic aldehydes with acetophenone has been established.

The method provided furano-chalcones with selectivities consistently above 90% within 2 h at 150 °C. Magnesium oxide proved to be an efficient and recyclable heterogeneous catalyst, maintaining activity up to the sixth reuse, as confirmed by FESEM and XRD characterization of fresh and spent material.

The combination of renewable feedstocks, recyclable catalysis and microwave heating enabled a highly efficient and environmentally benign synthesis. Preliminary antiviral assays indicated promising activity, particularly for compound **3c** against *herpes simplex virus* type 2, and further biological studies are required. Future studies will be focused on the characterization of the antiviral potential of compound **3c** and newly synthesized analogues against human herpetic viruses. Overall, these results demonstrate that the solvent-free, MW-assisted protocol not only provides high selectivity, but also enhances energy efficiency, eliminates hazardous reagents and auxiliary substances, offering reduced waste production, improved efficiency, and broad substrate applicability, aligning with key principles of green chemistry.

Author contributions

L. T.: synthesis, purification, and writing – original draft. F. V.: chemical analyses and writing – original draft. E. C. G.: conceptualization, supervision, and writing – review & editing. S. T.: data curation. I. A.: biological assays and writing – original draft. D. L.: supervision and writing – review & editing. M. D.: data curation and writing – review & editing. G. C.: supervision and writing – review & editing. M. M.: conceptualization, catalyst characterization, supervision, and writing – review & editing.

Conflicts of interest

There are no conflicts to declare.

Data availability

The data underlying this study are available from the corresponding authors upon reasonable request.

Supplementary information (SI) is available. See DOI: https://doi.org/10.1039/d5gc06471f.

Acknowledgements

References

1 M. Di Russo, D. Zjalic, G. S. Lombardi, A. Perilli, G. Congedo, S. Daugbjerg and C. Cadeddu, *Eur. J. Public Health*, 2023, **33**, ckad160.1182.
2 L. Belkhir and A. Elmeligi, *J. Cleaner Prod.*, 2019, **214**, 185–194.
3 A. Booth, A. Jager, S. D. Faulkner, C. C. Winchester and S. E. Shaw, *Int. J. Environ. Res. Public Health*, 2023, **20**, 3206.
4 M. Milanesi, A. Runfola and S. Guercini, *J. Cleaner Prod.*, 2020, **261**, 121204.
5 N. A. A. Elkanzi, H. Hrichi, R. A. Alolayan, W. Derafa, F. M. Zahou and R. B. Bakr, *ACS Omega*, 2022, **7**, 27769–27786.
6 H. A. Jasim, L. Nahar, M. A. Jasim, S. A. Moore, K. J. Ritchie and S. D. Sarker, *Biomolecules*, 2021, **11**, 1203.
7 D. Elkhalifa, I. Al-Hashimi, A.-E. Al Moustafa and A. Khalil, *J. Drug Targeting*, 2021, **29**, 403–419.
8 M. H. Nematollahi, M. Mehrabani, Y. Hozhabri, M. Mirtajaddini and S. Iravani, *Heliyon*, 2023, **9**, e20428.
9 M. Das and K. Manna, *J. Toxicol.*, 2016, **2016**, 7651047.
10 T. Zhang, C. Yuan, Q. Zhou, H. Xin, Y. Liu, J. Tian, T. Deng and W. Xue, *J. Saudi Chem. Soc.*, 2023, **27**, 101773.
11 A. A. WalyEldeen, S. Sabet, H. M. El-Shorbagy, I. A. Abdelhamid and S. A. Ibrahim, *Chem.-Biol. Interact.*, 2023, **369**, 110297.
12 T. Constantinescu and C. N. Lungu, *Int. J. Mol. Sci.*, 2021, **22**, 11306.
13 B. Salehi, C. Quispe, I. Chamkhi, N. El Omari, A. Balahbib, J. Sharifi-Rad, A. Bouyahya, M. Akram, M. Iqbal, A. O. Docea, C. Caruntu, G. Leyva-Gómez, A. Dey,

M. Martorell, D. Calina, V. López and F. Les, *Front. Pharmacol.*, 2021, **11**, 592654.

14 M. Mellado, R. Sariego-Kluge, F. Valdés-Navarro, C. González, R. Sánchez-González, N. Pizarro, J. Villena, C. Jara-Gutierrez, C. Cordova, M. A. Bravo and L. F. Aguilar, *Spectrochim. Acta, Part A*, 2023, **291**, 122332.

15 S. Wangngae, K. Chansaenpak, J. Nootem, U. Ngivprom, S. Aryamueang, R.-Y. Lai and A. Kamkaew, *Molecules*, 2021, **26**, 2979.

16 K. S. Arias, M. J. Climent, A. Corma and S. Iborra, *Top. Catal.*, 2016, **59**, 1257–1265.

17 A. Kelloway and P. Daoutidis, *Ind. Eng. Chem. Res.*, 2014, **53**, 5261–5273.

18 J. B. Sperry and D. L. Wright, *Curr. Opin. Drug Discovery Dev.*, 2005, **8**, 723–740.

19 A. M. Abdula, G. L. Mohsen, B. H. Jasim, M. S. Jabir, A. I. R. Rushdi and Y. Baqi, *Heliyon*, 2024, **10**, e32257.

20 R. Zhang, F. Hong, M. Zhao, X. Cai, X. Jiang, N. Ye, K. Su, N. Li, M. Tang, X. Ma, H. Ni, L. Wang, L. Wan, L. Chen, W. Wu and H. Ye, *ACS Med. Chem. Lett.*, 2022, **13**, 560–569.

21 H. B. Thapa, N. Bajracharya, S. Thapa and G. B. Bajracharya, *Asian J. Chem.*, 2022, **34**, 2935–2941.

22 S. Narwal, B. Devi, T. Dhanda, S. Kumar and S. Tahlan, *J. Mol. Struct.*, 2024, **1303**, 137554.

23 X. Liu, Y. Chen, Y. Deng, C. Xiao, S. Luan and Q. Huang, *J. Agric. Food Chem.*, 2022, **70**, 1766–1775.

24 N. Z. Ismail, M. Khairuddean, M. Al-Anazi and H. Arsad, *Naunyn-Schmiedeberg's Arch. Pharmacol.*, 2024, **397**, 8993–9006.

25 J. Suresh, S. C. Baek, S. P. Ramakrishnan, H. Kim and B. Mathew, *Int. J. Biol. Macromol.*, 2018, **108**, 660–664.

26 A. Datta, S. Walia and B. S. Parmar, *J. Agric. Food Chem.*, 2001, **49**, 4726–4731.

27 *Comprehensive Organic Name Reactions and Reagents*, John Wiley & Sons, Ltd, 2010, pp. 660–664.

28 G. Rajendran, D. Bhanu, B. Aruchamy, P. Ramani, N. Pandurangan, K. N. Bobba, E. J. Oh, H. Y. Chung, P. Gangadaran and B.-C. Ahn, *Pharmaceuticals*, 2022, **15**, 1250.

29 E. J. Diana, U. S. Kanchana, T. V. Mathew and G. Anilkumar, *Appl. Organomet. Chem.*, 2020, **34**(12), e5987.

30 G. D. Yadav and D. P. Wagh, *ChemistrySelect*, 2020, **5**, 9059–9085.

31 V. K. Díez, C. R. Apesteguía and J. I. Di Cosimo, *J. Catal.*, 2006, **240**, 235–244.

32 B. Roy, A. S. Roy, A. B. Panda, Sk. M. Islam and A. P. Chattopadhyay, *ChemistrySelect*, 2016, **1**, 4778–4784.

33 M. Chinthala, A. Balakrishnan, P. Venkataraman, V. Manaswini Gowtham and R. K. Polagani, *Environ. Chem. Lett.*, 2021, **19**, 4415–4454.

34 B. A. Roberts and C. R. Strauss, *Acc. Chem. Res.*, 2005, **38**, 653–661.

35 A. de la Hoz, Á. Díaz-Ortiz and A. Moreno, *Chem. Soc. Rev.*, 2005, **34**, 164–178.

36 K. Martina, G. Cravotto and R. S. Varma, *J. Org. Chem.*, 2021, **86**, 13857–13872.

37 F. Bucciol, E. C. Gaudino, A. Villa, M. C. Valsania, S. Bellomi, S. Tabasso, G. Cravotto and M. Manzoli, *ChemCatChem*, 2025, **17**, e202500268.

38 F. Bucciol, E. C. Gaudino, A. Villa, M. C. Valsania, G. Cravotto and M. Manzoli, *ChemPlusChem*, 2023, **88**, e202300017.

39 M. R. Sazegar, S. Mahmoudian, A. Mahmoudi, S. Triwahyono, A. A. Jalil, R. R. Mukti, N. H. N. Kamarudin and M. K. Ghoreishi, *RSC Adv.*, 2016, **6**, 11023–11031.

40 A. DeVierno Kreuder, T. House-Knight, J. Whitford, E. Ponnusamy, P. Miller, N. Jesse, R. Rodenborn, S. Sayag, M. Gebel, I. Aped, I. Sharfstein, E. Manaster, I. Ergaz, A. Harris and L. Nelowet Grice, *ACS Sustainable Chem. Eng.*, 2017, **5**, 2927–2935.

41 R. Francese, A. Civra, M. Donalisio, N. Volpi, F. Capitani, S. Sottemano, P. Tonetto, A. Coscia, G. Maiocco, G. E. Moro, E. Bertino and D. Lembo, *PLoS Neglected Trop. Dis.*, 2020, **14**, e0008713.

42 T. Ma, P. Yang, I. Dammann, Z. Lin, A. S. Mougharbel, M.-X. Li, F. Adăscăliței, R. Mitea, C. Silvestru, C. Thorstenson, M. S. Ullrich, K. Cseh, M. A. Jakupec, B. K. Keppler, M. Donalisio, R. Cavalli, D. Lembo and U. Kortz, *Inorg. Chem.*, 2020, **59**, 2978–2987.

43 T. Selvamani, A. Sinhamahapatra, D. Bhattacharjya and I. Mukhopadhyay, *Mater. Chem. Phys.*, 2011, **129**, 853–861.

44 Y. Qu, W. Zhou, Z. Ren, K. Pan, C. Tian, Y. Liu, S. Feng, Y. Dong and H. Fu, *Eur. J. Inorg. Chem.*, 2012, **2012**, 954–960.

45 A. H. Jadhav, D. Prasad, H. S. Jadhav, B. M. Nagaraja and J. G. Seo, *Energy*, 2018, **160**, 635–647.

46 D. B. Bawiskar, P. M. Srinivasappa, B. L. Nikam, S. Kusuma, N. K. Chaudhari and A. H. Jadhav, *New J. Chem.*, 2024, **48**, 2448–2463.

47 A. B. Patil and B. M. Bhanage, *Catal. Commun.*, 2013, **36**, 79–83.

48 X. Qi, X. Yan, W. Peng, J. Zhang, Y. Tong, J. Li, D. Sun, G. Hui and J. Zhang, *New J. Chem.*, 2019, **43**, 4698–4705.

49 G. D. Yadav and A. R. Yadav, *RSC Adv.*, 2014, **4**, 63772–63778.

50 U. G. M. Ekanayake, H. Weerathunga, J. Weerasinghe, E. R. Waclawik, Z. Sun, J. M. MacLeod, A. P. O'Mullane and K. (Ken) Ostrikov, *Sustainable Mater. Technol.*, 2022, **32**, e00394.

51 M. Wang, Z. Shi, Z. Yu, S. Li, Z. Zhang and F. Wang, *ChemCatChem*, 2025, **17**, e202400441.

52 Z. Khademi and M. M. Heravi, *Tetrahedron*, 2022, **103**, 132573.

53 S. Subbiah, S. P. Simeonov, J. M. S. S. Esperança, L. P. N. Rebelo and C. A. M. Afonso, *Green Chem.*, 2013, **15**, 2849–2853.

54 S. Liu, Y. Zhu, Y. Liao, H. Wang, Q. Liu, L. Ma and C. Wang, *Appl. Energy Combust. Sci.*, 2022, **10**, 100062.

55 Y. Hu, S. Li, X. Zhao, C. Wang, X. Zhang, J. Liu, L. Ma, L. Chen and Q. Zhang, *Catal. Commun.*, 2022, **172**, 106532.

56 G. Cravotto and D. Carnaroglio, *Microwave Chemistry*, De Gruyter, 2017.

57 C. Chen, M. Lv, H. Hu, L. Huai, B. Zhu, S. Fan, Q. Wang and J. Zhang, *Adv. Mater.*, 2024, **36**, 2311464.

58 Q.-S. Kong, X.-L. Li, H.-J. Xu and Y. Fu, *Fuel Process. Technol.*, 2020, **209**, 106528.

59 F. Mariatti, I. Miletto, G. Paul, L. Marchese, S. Tabasso, M. Manzoli, G. Cravotto and E. Gianotti, *RSC Adv.*, 2020, **10**, 38578–38582.

60 S. Halder, S.-C. Chen, C.-H. Hsiao, F.-C. Chou and Y.-C. Lin, *Biomass Bioenergy*, 2025, **197**, 107842.

61 A. Messori, A. Fasolini and R. Mazzoni, *ChemSusChem*, 2022, **15**, e202200228.

62 Z.-H. Xie, H.-Y. Zhou, C.-S. He, Z.-C. Pan, G. Yao and B. Lai, *Chem. Eng. J.*, 2021, **414**, 128713.

63 M. Xu and M. Wei, *Adv. Funct. Mater.*, 2018, **28**, 1802943.

64 W. Y. Hernández, J. Lauwaert, P. Van Der Voort and A. Verberckmoes, *Green Chem.*, 2017, **19**, 5269–5302.

65 D. M. P. Mingos and D. R. Baghurst, *Chem. Soc. Rev.*, 1991, **20**, 1.

66 M. Tsuji, M. Hashimoto, Y. Nishizawa, M. Kubokawa and T. Tsuji, *Chem. – Eur. J.*, 2005, **11**, 440–452.

67 T. Ji, Z. Yang, S. Song, T. Zhou, L. Mu, X. Lu and J. Zhu, *Chem. Eng. Sci.*, 2022, **262**, 118035.

68 H. Shi, K. Huang, Y. Liu and D. Gou, *J. Phys. Chem. B*, 2023, **127**, 970–979.

69 A. L. Gajengi, T. Sasaki and B. M. Bhanage, *Adv. Powder Technol.*, 2017, **28**, 1185–1192.

70 D. Fan, X. Dong, Y. Yu and M. Zhang, *Phys. Chem. Chem. Phys.*, 2017, **19**, 25671–25682.

71 M. Sassi and K. M. Rosso, *Phys. Chem. Chem. Phys.*, 2024, **26**, 2269–2276.

72 Z. Wang, P. Fongarland, G. Lu, W. Zhan and N. Essayem, *J. Rare Earths*, 2018, **36**, 359–366.

73 D. T. Ngo, Q. Tan, B. Wang and D. E. Resasco, *ACS Catal.*, 2019, **9**, 2831–2841.

74 B. M. Choudary, M. L. Kantam, K. V. S. Ranganath, K. Mahendar and B. Sreedhar, *J. Am. Chem. Soc.*, 2004, **126**, 3396–3397.

75 M. Zhou, L. A. Curtiss and R. S. Assary, *Chem. Res. Chin. Univ.*, 2023, **39**, 1010–1016.

76 J. Lichtenberger, S. Hargroveleak and M. Amiridis, *J. Catal.*, 2006, **238**, 165–176.

77 I. Abid, W. Moslah, S. Cojean, N. Imbert, P. M. Loiseau, A. Chamayou, N. Srairi-Abid, R. Calvet and M. Baltas, *Molecules*, 2024, **29**, 1819.

78 T. V. T. Phan, C. Gallardo and J. Mane, *Green Chem.*, 2015, **17**, 2846–2852.

79 K. V. Aken, L. Strekowski and L. Patiny, *Beilstein J. Org. Chem.*, 2006, **2**, 2–3.

80 A. E. Aiwonegbe and J. U. Iyasele, *ChemSearch J.*, 2024, **15**, 1–7.

81 M. G. T. C. Ribeiro, D. A. Costa and A. A. S. C. Machado, *Green Chem. Lett. Rev.*, 2010, **3**, 149–159.

82 E. Khusnutdinova, Z. Galimova, A. Lobov, I. Baikova, O. Kazakova, H. N. T. Thu, N. V. Tuyen, Y. Gatilov, R. Csuk, I. Serbian and S. Hoenke, *Nat. Prod. Res.*, 2022, **36**, 5189–5198.

83 A. Phrutivorapongkul, V. Lipipun, N. Ruangrungsi, K. Kirtikara, K. Nishikawa, S. Maruyama, T. Watanabe and T. Ishikawa, *Chem. Pharm. Bull.*, 2003, **51**, 187–190.

84 W. Zhang, Z. Ma, X. Han and G. Li, *Fitoterapia*, 2024, **178**, 106151.

85 V. Patil, S. A. Patil, R. Patil, A. Bugarin, K. Beaman and S. A. Patil, *Med. Chem.*, 2019, **15**, 150–161.

86 R. Marinov, N. Markova, S. Krumova, K. Yotovska, M. M. Zaharieva and P. Genova-Kalou, *Antivir. Prop. Chalcones Their Synth. Deriv. Mini Rev.*, 2020, **67**, 325–337.

87 L. K. M. Kirton, N. N. Yousef, G. D. Parks and O. Phanstiel IV, *Biomolecules*, 2025, **15**, 1285.

88 P. Hariyono, J. C. Kotta, C. F. Adhipandito, E. Aprilianto, E. J. Candaya, H. A. Wahab and M. Hariono, *Appl. Biol. Chem.*, 2021, **64**, 69.

89 A. B. Musatat, T. Durmuş and A. Atahan, *Arch. Biochem. Biophys.*, 2024, **761**, 110171.

90 J.-H. Wu, X.-H. Wang, Y.-H. Yi and K.-H. Lee, *Bioorg. Med. Chem. Lett.*, 2003, **13**, 1813–1815.